Geosci. Model Dev. Discuss., 7, 7461–7503, 2014
www.geosci-model-dev-discuss.net/7/7461/2014/
doi:10.5194/gmdd-7-7461-2014

Geoscientific Model Development Discussions
Open Access

Carbon isotopes in the ocean model of the Community Earth System Model (CESM1)

A. Jahn[1], K. Lindsay[1], X. Giraud[2,3], N. Gruber[3], B. L. Otto-Bliesner[1], Z. Liu[4], and E. C. Brady[1]

[1]National Center for Atmospheric Research, Climate and Global Dynamics Division, Boulder, CO, USA
[2]Aix Marseille Université, CNRS, IRD, Collège de France, CEREGE UM34, Aix en Provence, France
[3]Environmental Physics Group, Institute of Biogeochemistry and Pollutant Dynamics, ETH Zürich, Zürich, Switzerland
[4]Department of Atmospheric and Oceanic Sciences, and Center for Climatic Research, University of Wisconsin – Madison, Madison, WI, USA

Received: 20 September 2014 – Accepted: 20 October 2014 – Published: 6 November 2014

Correspondence to: A. Jahn (ajahn@ucar.edu)

Published by Copernicus Publications on behalf of the European Geosciences Union.

Abstract

Carbon isotopes in the ocean are frequently used as paleo climate proxies and as present-day geochemical ocean tracers. In order to allow a more direct comparison of climate model results with this large and currently underutilized dataset, we added a carbon isotope module to the ocean model of the Community Earth System Model (CESM), containing the cycling of the stable isotope ^{13}C and the radioactive isotope ^{14}C. We implemented the ^{14}C tracer in two ways: in the "abiotic" case, the ^{14}C tracer is only subject to air–sea gas exchange, physical transport, and radioactive decay, while in the "biotic" version, the ^{14}C additionally follows the ^{13}C tracer through all biogeochemical and ecological processes. Thus, the abiotic ^{14}C tracer can be run without the ecosystem module, requiring significantly less computational resources. The carbon isotope module calculates the carbon isotopic fractionation during gas exchange, photosynthesis, and calcium carbonate formation, while any subsequent biological process such as remineralization as well as any external inputs are assumed to occur without fractionation. Given the uncertainty associated with the biological fractionation during photosynthesis, we implemented and tested three parameterizations of different complexity. Compared to present-day observations, the model is able to simulate the oceanic ^{14}C bomb uptake and the ^{13}C Suess effect reasonably well compared to observations and other model studies. At the same time, the carbon isotopes reveal biases in the physical model, for example a too sluggish ventilation of the deep Pacific Ocean.

1 Introduction

A large fraction of paleoclimatic reconstructions are based on isotopic measurements (e.g. Petit et al., 1999; McDermott, 2004; Curry and Oppo, 2005; Polka et al., 2013), yet there are many uncertainties associated with the interpretation of these records in terms of physical climate variables such as temperature, precipitation, and ocean

GMDD
7, 7461–7503, 2014

circulation rates. More direct comparisons of paleo data with climate models would therefore be beneficial, both to test the interpretation of the isotopic proxy data and to allow for better comparisons of model simulations with proxy data. Furthermore, many isotope tracers are currently being measured in the ocean, and including them in ocean models can help us better understand the ocean circulation and diagnose model biases (e.g. Matsumoto et al., 2004). For all of these reasons, we have added a carbon isotope module to the ocean model of the Community Earth System Model (CESM) (Hurrell et al., 2013).

Carbon has two stable isotopes, ^{12}C and ^{13}C. More than 98.9 % of carbon on earth is ^{12}C, while ^{13}C makes up most of the remaining 1 %. The radioactive carbon isotope ^{14}C, also called radiocarbon, is present only in trace amounts (approximately 1×10^{-10}% of all carbon) and has a half-life of 5730 years (Godwin, 1962). Radiocarbon is a useful tracer to evaluate the ventilation of the deep ocean because it acts as a clock, measuring the time since water was last in contact with the atmosphere (e.g. Toggweiler et al., 1989; Orr, 2002; Meissner et al., 2003; Waugh et al., 2003; Key et al., 2004; Doney et al., 2004; Matsumoto et al., 2004; Meissner, 2007; Bardin et al., 2014). Because of the atmospheric nuclear weapons tests in the 1950s and 1960s and the well-known input-function of radiocarbon during this time, radiocarbon is also useful to evaluate the recent penetration of anthropogenic carbon into the ocean (e.g. Graven et al., 2012). Furthermore, oceanic radiocarbon has been used to determine the mean gas exchange velocity used in ocean models (e.g. Wanninkhof, 1992; Sweeney et al., 2007; Naegler et al., 2006; Naegler, 2009). Oceanic $\delta^{13}C$ has been used in paleoclimate studies as a tracer of the ocean circulation (e.g. Marchal et al., 1998; Curry and Oppo, 2005; Crucifix, 2005), to calculate the uptake of anthropogenic carbon dioxide (e.g. Keeling et al., 1980; Quay et al., 1992; Gruber et al., 1999; Sonnerup et al., 1999; Gruber and Keeling, 2001), and to diagnose biases in marine ecosystem models (e.g. Schmittner et al., 2013).

We added the carbon isotopes to the code in a way that they follow the cycling of total carbon through all ecosystem and physical/chemical processes. In this biotic

GMDD
7, 7461–7503, 2014

formulation, a new ^{13}C and ^{14}C state variable was added to each carbon-bearing state variable resulting in a total of 14 new state variables. For ^{14}C, we also added the option of a simplified representation, where the isotope is only subject to the main chemical and physical processes during gas exchange and decay, but does not cycle through the ecosystem. This abiotic formulation of ^{14}C was implemented based on the Ocean Carbon Model Intercomparison Project Phase 2 (OCMIP-2) protocol (Orr et al., 2000).

Abiotic radiocarbon had been added previously to the NCAR ocean model (in NCOM1.4, Orr, 2002, and POP1/CCSM3, Graven et al., 2012), and biotic ^{13}C was implemented into the ecosystem model of the CCSM3 by X. Giraud and N. Gruber in 2009–2010. However, neither development was ever added to the trunk of the ocean model code of the CESM, so it was not maintained as the model evolved over the years and consequently none of these implementations still work in the current ocean model of the CESM. The current developments have been added to the code trunk of the current ocean model of CESM in order to increase the chances of maintaining these developments as the model continues to evolve. By including carbon isotopes in the ocean model of the CESM1, the CESM1 joins the community of other comprehensive ocean general circulation models that include abiotic radiocarbon and/or biotic ^{13}C in the ocean (e.g. MoBidiC, Crucifix, 2005, PISCES, Tagliabue and Bopp, 2008, CM2Mc ESM, Galbraith et al., 2011, HAMOCC2s, Hesse et al., 2011, and UVic ESCM, e.g. Meissner et al., 2003; Schmittner et al., 2013).

As a reference for future studies using these new capabilities, we describe the model used (Sect. 2), describe the details of the implementation of the abiotic and biotic carbon isotopes (Sect. 3), compare the simulated carbon isotope fields to observational data to show the general performance of the model (Sect. 4), and mention changes in the most recent version of the CESM as they relate to the carbon isotopes (Sect. 5).

GMDD
7, 7461–7503, 2014

2 Model

This work was done using the Community Earth System Model (CESM) (Hurrell et al., 2013), versions 1.0.5. It has been adapted to CESM1.2 (see Sect. 5) and is targeted for public release in 2015 as part of CESM1.3. The CESM is a fully-coupled climate model with components for the atmosphere, land, river runoff, sea ice, ocean and ice sheets, coupled by a coupler. Its components and simulations have been described in a large collection of articles, many of them contained in a special collection in the Journal of Climate (http://journals.ametsoc.org/page/CCSM4/CESM1). The simulations analyzed here were performed using the ocean model coupled to data models for the atmosphere, the land, the sea ice, and the river routing, using repeated normal year forcing from CORE-II (Large and Yeager, 2009). The ocean model was run at a nominal 3° horizontal resolution with 60 vertical levels, which is the low-resolution configuration of the ocean model (Shields et al., 2012).

3 Carbon isotope implementation

The carbon isotopes were added as optional passive tracers, with the biotic and abiotic implementations as two different options that can be set at the compilation and build time. The abiotic ^{14}C can be run with or without the ocean ecosystem model, while the biotic ^{13}C and ^{14}C require the ocean ecosystem model to be turned on.

3.1 Abiotic ^{14}C

In this implementation, $DI^{14}C$ is the model's normalized concentration of total dissolved inorganic ^{14}C, following the OCMIP2 protocol (Orr et al., 2000). $DI^{14}C$ is used as normalized concentration in order to minimize the numerical error of carrying very small numbers. The normalization is done by dividing the real $DI^{14}C$ by the standard ratio of $^{14}C/^{12}C = 1.176 \times 10^{-12}$ (Karlen et al., 1968). To obtain comparable $DI^{14}C$ values as measured, we multiply the simulated $DI^{14}C$ by this scaling factor of 1.176×10^{-12}. Since

GMDD
7, 7461–7503, 2014

the abiotic radiocarbon is designed to be run without the ocean ecosystem active, we also carry an abiotic $DI^{12}C$ tracer to calculate the isotope ratio $^{14}R = DI^{14}C/DI^{12}C$. For comparisons with observations, we calculate $\Delta^{14}C$ as a diagnostic variable:

$$\Delta^{14}C = (^{14}R - 1) \cdot 1000. \quad (1)$$

By construction, the abiotic $DI^{12}C$ and $DI^{14}C$ tracers only depend on the solubility of carbon in seawater and neglect all biological activity. The error in $\Delta^{14}C$ due to neglecting biology activity has been estimated to be on the order of 10 % (Fiadiero, 1982).

Note that we do not multiply ^{14}R by $^{14}R_{std}$ in Eq. (1), as we are using a normalized $DI^{14}C$ (following Orr et al., 2000). Given that this abiotic implementation does not account for the fractionation during gas exchange, we do not apply the correction for fractionation that is commonly applied to observational measurements of $^{14}C/^{12}C$ ratios (as well as for the biotic ^{14}C implementation, see Eq. (27) in Sect. 3.2.4). The simulated abiotic $\Delta^{14}C$ is therefore directly comparable to observed data reported as $\Delta^{14}C$ (see Toggweiler et al., 1989, for more details).

3.1.1 Surface fluxes

We follow the abiotic OCMIP-2 protocol (Orr et al., 2000) for most of the implementation of the abiotic radiocarbon surface fluxes, with the following notable differences:

- We use a coefficient a of 0.31 cm h^{-1} (Wanninkhof, 1992) instead of 0.337 cm h^{-1} as used in OCMIP-2. This is higher than what most recent estimates suggest (e.g., Sweeney et al., 2007; Naegler et al., 2006; Naegler, 2009; Graven et al., 2012), but makes it consistent with the gas-transfer formulation used in other parts of the CESM.

- We use the daily mean of the squared 10 m windspeed (either from the prescribed CORE-II forcing or from the coupled atmospheric model) instead of the climatology of the squared monthly average of the instantaneous SSMI velocity and its instantaneous variance as used in OCMIP-2.

GMDD
7, 7461–7503, 2014

– We use the daily mean of the ice fraction and atmospheric pressure (either from the data models or the coupled sea ice and atmosphere models) instead of the monthly averaged climatology used in OCMIP-2.

– We use a constant reference value (1944 µmol m^{-3}) for the virtual fluxes of abiotic radiocarbon, rather than an annually updated average of the surface DI^{14}C as suggested in OCMIP-2. This is done to conserve total ^{14}C in the model (in absence of radioactive decay).

To compute the partial pressure of CO_2 from the abiotic DI^{12}C, we require an estimate of surface alkalinity. We follow again OCMIP-2, i.e., we estimate surface alkalinity (Alk) by scaling the ocean mean alkalinity, Alkbar = 2310 µmol kg^{-1} with sea-surface salinity, SSS, i.e.,

$$\mathrm{Alk} = \mathrm{Alkbar} \cdot \rho_{\mathrm{sw}} \cdot \mathrm{SSS} / S_{\mathrm{Ref}} \quad (2)$$

with $S_{\mathrm{Ref}} = 34.7$ and $\rho_{\mathrm{sw}} = 4.1/3.996\,\mathrm{g\,cm^{-3}}$ (these two are constants in the CESM). We alter this calculation in the Baltic Sea and the Black Sea to avoid unrealistic Alkalinity values, following the procedure developed by K. Lindsay for creating initial conditions for the marine ecosystem model: in the Black Sea, the surface alkalinity is independent of SSS: alkalinity = $3300 \cdot \rho_{\mathrm{sw}}$. In the Baltic Sea, we calculate Alkalinity depending on the surface salinity, with Alkalinity = $119 + 196 \cdot$SSS when SSS is equal to or below 7.3, and Alkalinity = $1237 + 43 \cdot$SSS when the SSS is above 7.3. The computation of pCO_2 also requires an assumption about the surface ocean concentrations of silicic acid and phosphate, for which we use OCMIP-2's global constants, i.e., 7.5 µmol kg^{-1} for silicic acid, $Si(OH)_4$, and 0.5 µmol kg^{-1} for phosphate, PO_4.

Air–sea gas exchange

As in OCMIP-2, the air–sea gas exchange flux of ^{12}C is calculated as

$$F = \mathrm{PV} \cdot (C_{\mathrm{sat}} - C_{\mathrm{surf}}) \quad (3)$$

GMDD
7, 7461–7503, 2014

with PV being the CO_2 gas transfer velocity (called the piston velocity) in $m\,s^{-1}$, calculated as

$$PV = (1 - aice) \cdot a \cdot u_{10}^2 \cdot (660.0/Sc_{CO_2})^{-1/2}. \quad (4)$$

The coefficient a is taken as $0.31\,cm\,h^{-1}$ as mentioned earlier, aice is the fraction of the ocean covered by sea ice, u_{10}^2 is the squared 10 m wind speed from the coupler, and Sc_{CO_2} is the Schmidt number of CO_2. Sc_{CO_2} is calculated as in the ecosystem model, following Wanninkhof (1992):

$$Sc_{CO_2} = 2073.1 + SST \cdot (-125.62 + SST \cdot (3.6276 + SST \cdot (-0.043219))). \quad (5)$$

C_{surf} in the gas flux calculation above is the surface aqueous CO_2 concentration in $mol\,m^{-3}$ (also called CO_2^*, which is the aqueous CO_2 concentration in $mol\,m^{-3}$ in the ocean in general). C_{sat} is the saturation concentration in $mol\,m^{-3}$, with $C_{sat} = CO_2^* + DCO_2^*$, and SST is the sea surface temperature. CO_2^* and DCO_2^* in turn are calculated by the carbonate solver from the ecosystem model, based on SST, SSS, ALK, PO_4, $Si(OH)_4$, pH, atmospheric pCO_2, atmospheric pressure, and the abiotic $DI^{12}C$ and $DI^{14}C$ concentration in the surface water.

As in OCMIP-2, we do not account for fractionation during gas exchange in this abiotic formulation, as the effect of isotopic fractionation is almost completely accounted for by the standard correction made when calculating $\Delta^{14}C$ from observations (see Toggweiler et al., 1989, for details).

The gas flux of the normalized abiotic $DI^{14}C$ is calculated as

$$F^{14} = PV \cdot (C_{sat} \cdot R^{14}C_{atm} - C_{surf} \cdot R^{14}C_{ocn}) \quad (6)$$

with

$$R^{14}C_{atm} = (1 + \Delta^{14}C_{atm}/1000) \quad (7)$$

GMDD
7, 7461–7503, 2014

and

$$R^{14}C_{ocn} = 1000 \cdot (DI^{14}C/DI^{12}C - 1). \quad (8)$$

The values of the atmospheric pCO_2 and $\Delta^{14}C_{atm}$ can be set to be constants or can be read in from a file. For atmospheric pCO_2, it can also be taken from the coupler, to ensure the use of a consistent atmospheric pCO_2 value across model components. Currently the code is set up to read in three files of $\Delta^{14}C_{atm}$ values, one each for the Northern Hemisphere, the equatorial region (20° N–20° S), and the Southern Hemisphere, in order to represent the spatial inhomogeneity of $\Delta^{14}C_{atm}$, for example after the atmospheric nuclear bomb tests.

Virtual fluxes

The CESM ocean model is a volume-conserving model where water fluxes at the surface (from precipitation, evaporation, and river input) are added as virtual fluxes. These virtual fluxes represent the dilution or concentration effect from adding or removing freshwater. For the abiotic carbon isotope tracers, we have a virtual $DI^{12}C$ and $DI^{14}C$ flux. As for salinity and for DIC in the ecosystem model, we use a constant surface reference $DI^{12}C$ and $DI^{14}C$ for the calculation of virtual fluxes in order to conserve tracers. The reference values are 1944 µmol m^{-3} for both $DI^{12}C$ and normalized $DI^{14}C$, the same as for DIC in the ecosystem model of CESM.

3.1.2 Interior processes

In the interior of the ocean, the only additional term to the transport of the tracers by the physical ocean model is the decay term for $DI^{14}C$, following the OCMIP-2 protocol.

$$d[DI^{12}C]/dt = L([DI^{12}C]) \quad (9)$$

and

$$d[DI^{14}C]/dt = L([DI^{14}C]) - \lambda \cdot [DI^{14}C] \quad (10)$$

GMDD
7, 7461–7503, 2014

with L being the 3-D transport operator and λ being the radioactive decay constant for ^{14}C in s^{-1}, using a half-life of 5730 years (Godwin, 1962):

$$\lambda = \ln(2)/(5730 \cdot 31\,556\,926). \quad (11)$$

The radiocarbon age (relative to AD 1950 = 0 yr BP) is calculated from $\Delta^{14}C$ following:

$$^{14}C_{age} = -5730/\ln 2 \times \ln(1 + \Delta^{14}C/1000) \quad (12)$$

5730 years / ln 2 = 8267 years is the mean life of ^{14}C, which differs from the often used mean-life of 8033 years (e.g. Stuiver and Polach, 1977), which is based on the earlier Libby half-life of 5568 (Libby, 1955).

3.2 Biotic ^{13}C and ^{14}C

In the biotic implementation of ^{13}C and ^{14}C, we use the ocean ecosystem model (e.g. Moore et al., 2013) to compute the carbon pools as well as all other biological variables (like silicic acid, alkalinity, etc). The ecosystem model currently has seven carbon pools: DIC, DOC (dissolved organic carbon), $CaCO_3$, diazotrophs, diatoms, small phytoplankton, and zooplankton. We carry passive tracers for each of these in the isotope-enabled version of the code. As ^{12}C makes up over 98 % of the carbon earth and does not fractionate, we assume that the ecosystem carries ^{12}C. This means that the isotope ratio R can be calculated as the ratio of the new isotopic carbon pools to the ecosystem carbon pools. As for the abiotic radiocarbon, we use scaled variables for ^{13}C and ^{14}C in order to minimize the numerical error of carrying very small numbers (particularly for ^{14}C). The scaling factor is the commonly used standard $^{iso}C/^{12}C$ for each isotope, i.e., 1.12372×10^{-8} for iso = ^{13}C (Craig, 1957) and 1.176×10^{-12} for iso = ^{14}C (Karlen et al., 1968). This means that we use $^{13}R_{Std} = 1$ and $^{14}R_{Std} = 1$ in the code, and that the model simulated isotopic carbon pools are multiplied by the respective scaling factor to compare them with observations.

GMDD
7, 7461–7503, 2014

In the biotic formulation, we account for the fractionation of ^{13}C and ^{14}C during gas exchange and during biological processes. The fractionation (ϵ) of ^{14}C is always twice that of ^{13}C, as all relevant processes have a mass-dependent fractionation for carbon (Bigeleisen, 1952; Craig, 1954). The isotopic fractionation ϵ is related to the fractionation factor α through:

$$\epsilon = (\alpha - 1) \cdot 1000. \quad (13)$$

As diagnostic variable, we compute the $\delta^{iso}C$ values by first computing the ratio $^{iso}R = DI^{iso}C/DIC$, and then using

$$\delta^{iso}C = (^{iso}R - 1) \cdot 1000. \quad (14)$$

As for the abiotic $\Delta^{14}C$ calculation in Eq. (1), we do not multiply by $^{iso}R_{Std}$ in the calculation of $\delta^{iso}C$ because we are using normalized $DI^{iso}C$.

3.2.1 Air–sea gas exchange of ^{13}C

The air–sea flux of ^{13}C is calculated based on Zhang et al. (1995):

$$F^{13} = PV \cdot \alpha_{aq_g} \cdot \alpha_k \cdot (R^{13}C_{atm} \cdot C_{sat} - R^{13}C_{DIC} \cdot C_{surf}/\alpha_{DIC_g}). \quad (15)$$

Here, C_{sat} and C_{surf} are obtained from the ecosystem model. $\alpha_k = -0.99919$ is the constant kinetic fractionation factor from Zhang et al. (1995) (with $\epsilon = -0.81$ and $\alpha = \epsilon/1000 + 1$). α_{aq_g} is the temperature (TEMP, in °C) dependent isotopic fractionation factor during gas dissolution, based on the equation for ϵ_{aq_g} from Zhang et al. (1995).

$$\epsilon_{aq_g} = -0.0049 \cdot TEMP - 1.31. \quad (16)$$

The temperature and carbonate fraction (f_{CO_3}) dependent fractionation factor (α_{DIC_g}) between total DIC and CO_2 is based on the empirical relationship for ϵ_{DIC_g} from Zhang

GMDD
7, 7461–7503, 2014

et al. (1995):

$$\epsilon_{\mathrm{DIC_g}} = 0.014 \cdot \mathrm{TEMP} \cdot f_{\mathrm{CO_3}} - 0.105 \cdot \mathrm{TEMP} + 10.53. \quad (17)$$

$R^{13}C_{atm}$ is the ^{13}C to ^{12}C ratio in atmospheric CO_2, calculated using the atmospheric $\delta^{13}C_{atm}$ record and $R_{atm} = 1 + \delta^{13}C_{atm}/1000$ (scaled by $^{13}R_{Std}$). The values of $\delta^{13}C_{atm}$ can be set to be a constant or it can be read in from a file. Currently $\delta^{13}C_{atm}$ is assumed to be well mixed globally, so only one global value is read in. With small code modifications globally inhomogeneous $\delta^{13}C_{atm}$ values can easily be read in instead. $R^{13}C_{DIC}$ is the ^{13}C to ^{12}C ratio of dissolved inorganic carbon, calculated from the simulated biotic DIC and DI^{13}C.

3.2.2 Virtual fluxes of ^{13}C

As stated in Sect. 3.1, we account for the dilution and concentration effect of surface freshwater fluxes in the model by adding a virtual flux, using a constant surface reference DI^{13}C (and DI^{14}C) of 1944 µmol m^{-3} for the calculation of virtual fluxes.

3.2.3 Biological fractionation of ^{13}C

The isotopic carbon-fixation by photosynthesis (photo^{13}C) is computed from the ^{12}C fixation during photosynthesis (photoC, from the ecosystem model), using

$$\mathrm{photo}^{13}\mathrm{C} = \mathrm{photoC} \cdot R_{\mathrm{p}} \quad (18)$$

with

$$R_{\mathrm{p}} = 1000 \cdot R_{\mathrm{CO_2^*}} / (\epsilon_{\mathrm{p}} + 1000) \quad (19)$$

and

$$R_{\mathrm{CO_2^*}} = R^{13}\mathrm{C_{DIC}} \cdot \alpha_{\mathrm{aq_g}} / \alpha_{\mathrm{DIC_g}}. \quad (20)$$

GMDD
7, 7461–7503, 2014

The strength of the biological fractionation of carbon during photosynthesis (ϵ_p), as well as the key controlling parameters, are still being debated in the literature (e.g. Keller and Morel, 1999). We therefore implemented three different parameterizations for ϵ_p to test the sensitivity of our results to the choice of biological fractionation.

The simplest model for ϵ_p by Rau et al. (1989) gives the same ϵ_p value for all types of autotrophs:

$$\epsilon_p = 1000 \cdot (\delta_{CO_2^*} - \delta_{C_p})/(1000 + \delta_{C_p}). \quad (21)$$

This relationship is based on the empirical relationship found by Rau et al. (1989) between the isotopic composition of the autotroph (δ_{C_p}) and CO_2^*:

$$\delta_{C_p} = -0.8 \cdot CO_2^* - 12.6, \quad (22)$$

limiting δ_{C_p} to values between −18 and −32 ‰ (Rau et al., 1989).

Laws et al. (1995) assumed that CO_2 enters the cell by diffusion and that the fractionation depends on the rate of photosynthesis, and therefore parameterized ϵ_p as a function of CO_2^* and the specific photosynthesis rate of each phytoplankton group (μ, in s^{-1}, calculated by the ecosystem model):

$$^{13}\epsilon_p = (\mu/CO_2^* \cdot 86\,400 - 0.371)/(-0.015). \quad (23)$$

Keller and Morel (1999) argued that only considering diffusive CO_2 transport into cells and assuming a linear relationship between ϵ_p and CO_2^* concentration and the specific growth rate (μ) does not agree with laboratory and field data, citing work by Sikes et al. (1980), Tortell et al. (1997), and Laws et al. (1997). Keller and Morel (1999) therefore proposed to use phytoplankton-type specific (constant) cell parameters (see Table 1) to compute the fractionation during photosynthesis:

$$^{13}\epsilon_p = \epsilon_{diff} + (C_{up}/(C_{up} + 1/var)) \cdot \delta_{d13C} + \theta \cdot (\epsilon_{fix} - \epsilon_{diff}) \quad (24)$$

GMDD
7, 7461–7503, 2014

where

$$\theta = (1 + (C_{up} - 1) \cdot var)/(1 + C_{up} \cdot var) \quad (25)$$

and

$$var = \mu/CO_2^* \cdot 1000 \cdot Qc/(cell_{permea} \cdot cell_{surf}) \quad (26)$$

with Qc being the cell carbon content, $cell_{permea}$ being the cell wall permeability to CO_2 (aq), $cell_{surf}$ being the surface areas of cells, C_{up} being the ratio of active carbon uptake to carbon fixation, ϵ_{fix} being a constant phytoplankton-type dependent fractionation effect of carbon fixation, $\epsilon_{diff} = 0.7$ representing the fractionation by diffusion (O'Leary, 1984), and $\delta_{d13C} = -9.0$ being the difference between the isotopic compositions of the external CO_2 and the organic matter pools (Goericke et al., 1994).

While the fractionation during calcium carbonate formation is much smaller than the fractionation during photosynthesis (Turner, 1982), we include a small constant fractionation of 2 ‰ for calcium carbonate formation, based on work by Ziveri et al. (2003).

3.2.4 Biotic ^{14}C

The ^{14}C air sea flux is calculated in the same way as shown in Eq. (15) for ^{13}C, but with the fractionation for ^{14}C being twice as large as for ^{13}C ($\epsilon_{14} = 2 \cdot \epsilon_{13}$, Zeebe and Wolf-Gladrow, 2001) and with $R^{14}C_{atm}$ and $R^{14}C_{DIC}$ instead of $R^{13}C_{atm}$ and $R^{13}C_{DIC}$. The biological fractionation is also the same as for ^{13}C, except that $\epsilon_{14} = 2 \cdot \epsilon_{13}$ everywhere in Sect. 3.2.3. The surface reference value for $DI^{14}C$ for the virtual flux calculation is 1944 µmol m^{-3}, the same as for $DI^{13}C$ (and $DI^{12}C$).

In contrast to ^{13}C, ^{14}C decays in all carbon pools, following the decay equation (see Eq. (11) in Sect. 3.1.2).

To compare the model simulated $\delta^{14}C$ values that we save as diagnostics (see Eq. 14) with published observations of $\Delta^{14}C$, we apply the same fractionation correction to it that is used for observations to convert $\delta^{14}C$ to $\Delta^{14}C$:

$$\Delta^{14}C = \delta^{14}C - 2(\delta^{13}C + 25)(1 + \delta^{14}C/1000). \quad (27)$$

GMDD
7, 7461–7503, 2014

In the following we always show $\Delta^{14}C$.

As for the abiotic ^{14}C implementation, the value of $\Delta^{14}C_{atm}$ can be set to be a constant or it can be read in from three files (one for the Northern Hemisphere, one for the equatorial region, and one for the Southern Hemisphere).

3.3 Ecosystem driver

We added an ecosystem driver (`ecosys_driver`) to the ocean model of the CESM in order to make it easier to expand the model to carry additional passive tracers that require variables from the ecosystem model, without adding these additional tracers to the ecosystem model itself. The ecosystem driver is structured similar to the `passive_tracers` subroutine that calls all passive tracer modules, but it handles only the passive tracers that use the ecosystem model (see Fig. 1). It is called from the `passive_tracers` subroutine, and determines how many ecosystem-related passive tracers the model carries based on the namelist options set at buildtime. It then calls all subroutines in the ecosystem model and the related tracer modules, after being called by passive tracers with the corresponding tracer indices. Variables computed in the ecosystem model but used by other modules are shared via the new `ecosys_share` module. Only the ecosystem model changes the value of the variables in `ecosys_share` at this point. Other modules currently only read them from there, but do not modify them. With this infrastructure in place, additional tracers can be easily added without changing the ecosystem model too much. The only changes to the ecosystem model should be the copying of ecosystem variables to `ecosys_share` if they need to be shared with a new module as well as potentially the addition of new definitions and calculations of derived ecosystem variables that are needed but that are not currently computed in the ecosystem model (or not present in the required format, i.e., defined as local 2-D variables instead of a global 3-D variable). Nitrogen isotopes in the ocean model have already been added using this infrastructure (S. Yang, personal communication, 2014).

GMDD
7, 7461–7503, 2014

4 Results

4.1 Simulations and spin-up

We have performed several simulations with the new carbon-isotope enabled model. As described in Sect. 2, we used the ocean-only version of the CESM1.0.5, at a nominal 3° horizontal resolution, forced by CORE-II climatological forcing (Large and Yeager, 2009). To spin up the carbon isotopes, we performed spin-up simulations that lasted several thousands of years. Radiocarbon takes a long time (5000–15 000 years, according to Orr et al., 2000) to equilibrate, due to the long timescale of deep ocean ventilation.

The abiotic radiocarbon has been spun-up for 10 000 years using an atmospheric CO_2 concentration of 284.7 ppm and a $\Delta^{14}C$ value of 0 ‰. The abiotic $DI^{14}C$ and $DI^{12}C$ were started from the standard ecosystem initial conditions, scaled to yield a global initial state of 0 ‰ $\Delta^{14}C$ (following Orr et al., 2000), in order to simplify early interpretation and code verification. After 10 000 simulated years, the models satisfies the OCMIP2 surface CO_2 flux criteria of less than 0.01 Pg C year^{-1}. In terms of the drift in $\Delta^{14}C$, 91 % of the ocean volume is spun-up to the OCMIP2 criteria of a drift of less than 0.001 ‰ year^{-1} (compared to the required 98 % for OCMIP2). Compared to the fully-spun-up solution (obtained using a new online Newton–Krylov method, manuscript in preparation by K. Lindsay, NCAR), differences are seen in the deep ocean only.

For the biotic carbon isotopes, we spun-up the carbon isotopes for 3560 years, starting from the initial conditions of the ecosystem model, scaled to give a $\delta^{13}C$ of 0 ‰ and a $\Delta^{14}C$ of −100 ‰. The atmospheric CO_2 concentration was set to 284.7 ppm, the atmospheric $\Delta^{14}C$ was set to 0 ‰, and the atmospheric $\delta^{13}C$ was set to −6.379 ‰. In order to study the different biological fractionation parameterizations, two additional 1000 year long spin-up simulations were branched from the first spin-up simulation at year 2560 and run to year 3560. After 3560 years, the surface CO_2 flux is well below the OCMIP2 criteria of less than 0.01 Pg C year^{-1}, and over 99.99 % of the ocean volume

GMDD
7, 7461–7503, 2014

show a drift of less than 0.001 ‰ year^{-1} in δ^{13}C. However, only 5 % of the ocean satisfies the OCMIP2 criteria of a drift of less than 0.001 ‰ year^{-1} for Δ^{14}C. If we weaken the criteria by an order of magnitude to less than 0.01 ‰ year^{-1}, 75 % of the ocean satisfy this new criteria for Δ^{14}C. Hence, when comparing the biotic and abiotic Δ^{14}C in the following, we need to consider that we are comparing an almost spun-up state in the abiotic Δ^{14}C to a still drifting state in the biotic Δ^{14}C. Due to the long time required to run the ocean model with the ecosystem and the biotic carbon isotopes (the 3560 years took over 4 months of constant running on a supercomputer), we are currently not able to run the biotic radiocarbon to equilibrium. In order to reach equilibrium in the future, a fast spin-up technique for the ecosystem model is currently in development by Keith Lindsay and will be applied to the biotic carbon isotopes when it is ready. We believe that for the purpose of this paper, which documents the implementation of the carbon isotopes in the model, the current spin-up is sufficient. For other science applications, however, the biotic radiocarbon would need to be spun up further in order to be fully trustworthy.

We then performed experiments from 1765 to 2008, with the initial conditions from the end of the spin-up simulations in year 3560 for the biotic carbon isotopes and in year 10 000 for the abiotic radiocarbon. The atmospheric CO_2, Δ^{14}C, and δ^{13}C was prescribed based on the OCMIP-2 files (Orr et al., 2000) up to 1989, and H. Graven's formulation of the global average for 1990–2008 (personal communication, 2012). The atmospheric state was the same repeating climatological CORE-II forcing as used for the spin-up, so changes related to warming or changes in the wind forcing over the 20th century are not included. At the same time, we continued the spin-up simulations for 243 years, so that we could remove the influence of a continuing drift on the radiocarbon results shown in Sect. 4.2.2. To investigate the influence of the net CO_2 uptake on the simulation results in the second part of the 20th century, we also performed sensitivity experiments where the atmospheric CO_2 was fixed at 1949 conditions, while $\Delta^{14}C_{atm}$ and $\delta^{13}C_{atm}$ changed as usual.

GMDD
7, 7461–7503, 2014

4.2 ^{14}C results

4.2.1 Simulated distributions of $\Delta^{14}C$

The radiocarbon simulation shows good agreement with the gridded GLODAP data for the 1990s (Key et al., 2004), reflecting the main features of the $\Delta^{14}C$ distribution: (i) at the surface (see Fig. 2) the model shows the observed M-shape of $\Delta^{14}C$ distribution, with the highest values in the relatively stable subtropical waters, intermediate values in the equatorial upwelling zone, and low values in the polar regions, where the residence time is short and sea ice limits the uptake of atmospheric $\Delta^{14}C$, with the overall lowest values in the Southern Ocean, where the upwelling of old, low $\Delta^{14}C$ waters further dilutes the surface waters. (ii) In the zonal mean (see Fig. 3), newly formed deepwater with high $\Delta^{14}C$ values can clearly be separated from old water masses with low $\Delta^{14}C$ values. (iii) In the depth profiles (see Fig. 4), it is obvious that the $\Delta^{14}C$ in the deep water decreases from the Atlantic Ocean over the Indian Ocean to the Pacific Ocean, which has the lowest $\Delta^{14}C$ values (i.e., oldest water). Consistently, the abiotic $\Delta^{14}C$ values are higher than the biotic $\Delta^{14}C$ values, but both show the same general features also shown in GLODAP (Key et al., 2004) and in the cruise data compiled by Schmittner et al. (2013) because their distribution is set mainly by the physical ocean simulation. The differences between the abiotic and biotic simulation due to biological effects is difficult to determine at this point, as the biotic simulation is much less spun-up than the abiotic simulation. This will be the topic of a future study when we can spin-up both radiocarbon implementations using a fast-spin up technique.

Above 1000 m, the depth structure of the simulated $\Delta^{14}C$ agrees reasonably well with observations, with the best agreement with the GLODAP $\Delta^{14}C$ in the upper 250 m of the Indian Ocean (see Fig. 4). The largest biases are found at depth below 1000 m (see Fig. 4), with the model showing $\Delta^{14}C$ values that are too negative (i.e., water that is too old). The largest bias is located in the deep Pacific, where the $\Delta^{14}C$ is up to 100 ‰ too negative (see Figs. 3 and 4). In terms of radiocarbon age, the maximum

GMDD
7, 7461–7503, 2014

bias in the deep Pacific is 1000 years compared to GLODAP, revealing that the deep Pacific Ocean in the model is not ventilated as much as it should be. This bias was also present in the ocean model of a previous version of the CESM, the CCSM3 (Graven et al., 2012), as well as in the nominal 1° resolution version of the current CESM1 ocean model (Bardin et al., 2014). Currently radiocarbon is being used to test improvements to the ocean model in the CESM, in order to improve this bias in future versions of the CESM (K. Lindsay, personal communication, 2014).

4.2.2 ^{14}C bomb inventory

The excess oceanic radiocarbon inventory is frequently being used to investigate the ocean uptake of anthropogenic carbon (e.g. Key et al., 2004; Graven et al., 2012) and to determine the mean gas exchange velocity used in ocean models (e.g. Wanninkhof, 1992; Sweeney et al., 2007; Naegler et al., 2006; Naegler, 2009). To establish how well the newly developed radiocarbon tracer compares to observations, we here compare the simulated excess radiocarbon inventory with observational estimates. The excess radiocarbon in the ocean includes change in the oceanic radiocarbon from the atmospheric nuclear bomb tests of the 1950s and 1960s, as well as from the Suess effect and changes in net CO_2 uptake, compared to the reference period of the 1940s, following Naegler (2009). In 1975, the excess radiocarbon inventory in the abiotic and biotic simulation is 286×10^{26} atoms ^{14}C and 291×10^{26} atoms ^{14}C, respectively. This lies within the range of observational estimates of the excess radiocarbon in 1975, which range from 225×10^{26} atoms ^{14}C to $314 \pm 35 \times 10^{26}$ atoms ^{14}C (see Table 2). It has been shown that the earlier estimates from Broecker et al. (1985, 1995) were high by about 25 % (e.g. Hesshaimer et al., 1994; Peacock, 2004; Sweeney et al., 2007), which suggests that the simulated values are probably on the high end of the observational range. One reason for this could be the choice of the coefficient $a = 0.31\,\mathrm{cm\,h^{-1}}$ in Eq. (3), which has been shown to be high (e.g. Sweeney et al., 2007; Naegler, 2009). Graven et al. (2012) showed that in the ocean model of the CCSM3, the simulated excess radiocarbon inventory was lower when a coefficient $a = 0.23\,\mathrm{cm\,h^{-1}}$ rather than

GMDD
7, 7461–7503, 2014

$a = 0.31\,\mathrm{cm\,h^{-1}}$ was used in Eq. (3). However, since $a = 0.31\,\mathrm{cm\,h^{-1}}$ is the parameter used in the CESM in general to compute air–sea gas fluxes, we did not change it here. For 1995, the excess radiocarbon inventory in the abiotic and biotic simulation are 372×10^{26} atoms ^{14}C and 384×10^{26} atoms ^{14}C, respectively, which agrees well with the observational estimates of 313–383 $\times 10^{26}$ atoms ^{14}C, particularly the most recent estimate from Naegler (2009) and the corrected estimates from Key et al. (2004) (see Table 2).

The natural radiocarbon inventory, before anthropogenic disturbances from the Suess effect and from increased oceanic net CO_2 uptake, has been estimated to be $19\,000 \pm 1200 \times 10^{26}$ atoms of ^{14}C (Naegler, 2009). In the model the inventory is within the error bar for the biotic model ($17\,959$–$17\,964 \times 10^{26}$ atoms of ^{14}C, depending on the biological fractionation used), and slightly lower for the abiotic model ($16\,730 \times 10^{26}$ atoms of ^{14}C). These inventories are calculated for years 3735–3744 of the control simulations, which corresponds to the same total runtime as years 1940–1949 in the 1765–2008 experiments, which were started from the control in year 3560. To calculate the early anthropogenic radiocarbon inventory present in the 1940s, we take the difference between the natural radiocarbon inventory in simulation years 3735–3744 (with constant atmospheric CO_2, $\Delta^{14}C$, and $\delta^{14}C$) and the inventory in the 1940s (with changing atmospheric CO_2, $\Delta^{14}C$, and $\delta^{14}C$ since 1765). By taking this difference between years of equal total runtime, we remove the impact of any remaining drift in $\Delta^{14}C$. We find an anthropogenic radiocarbon inventory of 20×10^{26} atoms of ^{14}C for the abiotic model and 5×10^{26} atoms of ^{14}C for the biotic model (independent of the biological fractionation used). Both of these anthropogenic radiocarbon inventories for the 1940s are within the error bar of the estimate of $4 \pm 20 \times 10^{26}$ of ^{14}C from Naegler (2009), with the biotic model giving a very good match.

Using sensitivity experiments from 1950–2008 with atmospheric CO_2 held constant at 1949 levels but normally increasing atmospheric $\Delta^{14}C$, we can calculate the impact of increased ocean uptake of anthropogenic CO_2 on the excess radiocarbon inventory: in 1975, the excess oceanic radiocarbon inventory relative to the 1940s due to

GMDD
7, 7461–7503, 2014

atmospheric $\Delta^{14}C$ changes alone (from the atmospheric bomb tests and the Suess effect) is 271×10^{26} atoms of ^{14}C for the abiotic model and 276×10^{26} atoms of ^{14}C for the biotic model, while for 1995 the numbers are 336×10^{26} atoms of ^{14}C and 348×10^{26} atoms of ^{14}C, respectively. This means that the increase in net CO_2 uptake contributed 15×10^{26} atoms of ^{14}C in 1975 and 36×10^{26} atoms of ^{14}C in 1995 compared to the 1940s (for both the abiotic and biotic models), which is 5 and 9 % of the total radiocarbon excess in these years. These changes are in excellent agreement with calculations from Naegler (2009), which showed an excess radiocarbon inventory in 1995 of $346 \pm 98 \times 10^{26}$ atoms ^{14}C due to atmospheric $\Delta^{14}C$ changes, and $27 \pm 9 \times 10^{26}$ atoms ^{14}C due to net CO_2 uptake. The percentage contribution of the net CO_2 uptake to the total radiocarbon excess was given as 3 % in 1975 and 8 % in 1995 in Naegler (2009), which again compares very well with our model simulation.

4.3 ^{13}C results

4.3.1 Simulated $\delta^{13}C$ and the impact of different biological fractionation parameterizations

In the literature, models of biological fractionation are still under debate (e.g. Keller and Morel, 1999). We therefore tested three different parameterizations of biological fractionation, to investigate the impact on the simulated $\delta^{13}C$ (as described in Sects. 3.2.3 and 4.1). As shown in Fig. 5a, the simulated globally averaged ϵ_p depth profiles differ when these different parameterizations are used, with ϵ_p values ranging from 15–30. By design, ϵ_p is the same for diatoms, diazotrophs, and small phytoplankton when using Rau et al. (1989), while ϵ_p shows large variations between species for the method of Keller and Morel (1999), due to the dependence on species-specific cell parameters (see Table 1). The method of Laws et al. (1995) leads to small differences between species in the surface ocean only. Below 200 m, only the ϵ_p following Rau et al. (1989) still changes with depth (see Fig. 5a), due to the sole dependence of ϵ_p on CO_2^* and the export of organic carbon and carbonates to depth.

GMDD
7, 7461–7503, 2014

The impact of the different biological fractionation choices on $\delta^{13}C_{DIC}$ is noticeable (see Fig. 5b), with the globally-averaged $\delta^{13}C_{DIC}$ based on ϵ_p from Rau et al. (1989) being larger below 150 m compared to the $\delta^{13}C_{DIC}$ from Laws et al. (1995) and Keller and Morel (1999), but slightly smaller at the surface. Despite the more complex formulation of ϵ_p in Keller and Morel (1999) compared to Laws et al. (1995) and the significantly different ϵ_p profiles, the resulting $\delta^{13}C_{DIC}$ from both methods is very similar and only differs slightly at depth (most notably between 150 and 2000 m). To compare the simulated $\delta^{13}C_{DIC}$ to the cruise data of $\delta^{13}C_{DIC}$ compiled by Schmittner et al. (2013), we re-gridded the model output to subsample the model at the same points as covered by the cruise data. The resulting globally-averaged depth profiles are shown in Fig. 5c, and are remarkably similar to the full globally-averaged model results in Fig. 5b. Both show the expected increase in $\delta^{13}C_{DIC}$ directly below the surface, due to the preferential uptake of the light isotope during photosynthesis, followed by the expected decrease of $\delta^{13}C_{DIC}$ with depth due to the remineralization of the isotopically light organic material back into the water column. The model simulated global depth-profile of $\delta^{13}C_{DIC}$ lies within the error range of ±0.2 ‰ around the cruise $\delta^{13}C_{DIC}$ data between the surface and 150 m and below 1000 m, but shows smaller $\delta^{13}C_{DIC}$ values than observed between 150 and 1000 m.

For individual basins, the model bias compared to the cruise data is smallest in the Atlantic, with the $\delta^{13}C_{DIC}$ based on the biological fractionation from Rau et al. (1989) almost entirely with in the uncertainty range of the data (see Fig. 5d). All three basins contribute to the bias seen between 150 and 2000 m in the global average, with the Indian Ocean contributing the most to this bias in the upper ocean and the Pacific Ocean contributing the most at intermediate depths (see Fig. 5c–f). In general, the model simulated $\delta^{13}C_{DIC}$ tends to be smaller than the observed $\delta^{13}C_{DIC}$. While the difference between the full global average in the model and the subset global average based on the cruise data locations is small, the difference between the total basin

GMDD
7, 7461–7503, 2014

average (shown as dashed lines in Fig. 5d–f) and the subset basin averages (shown as solid lines) is larger for the individual basins.

At the surface, the simulated $\delta^{13}C_{DIC}$ values show a systematic bias in that they are generally larger than the observational data suggests, but the same general spatial pattern is visible (see Fig. 6). While both gas-exchange and biological process are important for the surface ocean $\delta^{13}C_{DIC}$ pattern (Schmittner et al., 2013), the details of the biological fractionation parameterizations appear to have a very small impact at the surface, as shown in the almost identical surface distributions from the model (see Fig. 6c–e). The zonal means of $\delta^{13}C_{DIC}$ from the different biological fractionation parameterizations on the other hand do show some small differences (see Fig. 7), with the biological fractionation from Rau et al. (1989) leading to the largest $\delta^{13}C_{DIC}$ values in all three ocean basins, while the fractionation based on Keller and Morel (1999) shows the lowest $\delta^{13}C_{DIC}$ values. Overall all three parameterizations lead to the expected pattern of high values of $\delta^{13}C_{DIC}$ in water that has recently been in contact with the surface (e.g., North Atlantic Deep Water) and low $\delta^{13}C_{DIC}$ values in water that has been out-of-contact with the atmosphere for a long period of time and has accumulated a large amount of remineralized (isotopically light) organic mater (e.g., in the deep Pacific).

We choose the biological formulation from Laws et al. (1995) as the default biological fractionation in our model, as it considers the growth rate of different species, but the differences in the simulated $\delta^{13}C_{DIC}$ compared to the more complex formulation from Keller and Morel (1999) is small. The other parameterizations of biological fractionation remain an option in the model that can be chosen at build time.

4.3.2 Oceanic surface ^{13}C Suess effect

The surface oceanic Suess effect, which is the decrease in the surface ocean $\delta^{13}C$ due to the penetration of carbon originating from the burning of fossil fuels, has been calculated from observational data as well as from other models that include ^{13}C, and it is

GMDD
7, 7461–7503, 2014

often used to derive the oceanic anthropogenic carbon uptake (e.g. McNeil et al., 2001; Tagliabue and Bopp, 2008). In our model simulation, the surface $\delta^{13}C$ change between 1975 and 1995 is −0.159 to −0.163 ‰ decade^{-1} (the range is for the different biological fractionations used). This compares well with other estimates of −0.171 ‰ decade^{-1} (Bacastow et al., 1996), −0.018 ‰ decade^{-1} (Gruber et al., 1999), −0.15 ‰ decade^{-1} (Sonnerup et al., 1999), and −0.174 ‰ decade^{-1} (Tagliabue and Bopp, 2008). As already shown by Quay et al. (1992) and Gruber et al. (1999), the surface ocean Suess effect is not uniform (see Fig. 8), and the model simulation of the spatial Suess effect agrees well with the model results of Tagliabue and Bopp (2008): the largest changes (i.e., most negative values in Fig. 8) occur in regions with little deep ventilation and therefore longer residence times of water at the surface (e.g., the subtropical gyres) while the smallest changes (i.e., least negative or zero in Fig. 8) occur in regions of reduced air–sea gas exchange (e.g., under sea ice), in regions with active deep convection (and therefore short residence times at the surface, e.g. around Antarctic), as well as in regions with upwelling (which dilutes the surface $\delta^{13}C$, for example off the west coast of South America).

Compared to the pre-industrial ocean, the total surface ocean ^{13}C Suess effect is −0.064 to −0.066 ‰ decade^{-1} for 1860–2000 (depending on the different fractionations), compared to −0.07 ‰ decade^{-1} found by Tagliabue and Bopp (2008). The fact that the simulated oceanic ^{13}C Suess effect calculated over different periods agrees reasonably well with other available estimates suggests that our model is able to simulate the change in the oceanic $\delta^{13}C$ inventory correctly, despite some mean biases in the distribution of $\delta^{13}C$ described and shown in Sect. 4.3.1.

5 Changes in CESM1.2

In CESM1.2, the ocean ecosystem model prescribes the input of nutrients and carbon by rivers, while in CESM1.0 rivers only added a virtual salt flux to the ocean. This means that for the biotic carbon isotope implementation in CESM1.2, we also need to

GMDD
7, 7461–7503, 2014

add an isotopic carbon flux. Based on published research, we assume that globally, the $\delta^{13}C = -10‰$ for $DI^{13}C$ (Mook, 1986; Raymond et al., 2004) and the $\delta^{13}C = -27.6‰$ for $DO^{13}C$ (Raymond et al., 2004). The river runoff values of $\Delta^{14}C$ for $DI^{14}C$ and $DO^{14}C$ use the following constant global values to multiply the normal carbon fluxes from rivers in the ecosystem model: $\Delta^{14}C = -50‰$ for $DO^{14}C$ and $\Delta^{14}C = \Delta^{14}C_{atm} - 50‰$ for $DI^{14}C$ (e.g. Mook, 1986; Raymond et al., 2004).

The other notable change in the ecosystem model in CESM1.2 compared to the CESM1.0 that affects the carbon isotopes is the addition of bottom sediment cells. In CESM1.0 everything in the bottom cell was remineralized, while in CESM1.2 sedimentary burial and denitrification losses are calculated based on empirical relations (Dunne et al., 2007; Bohlen et al., 2012; Soetaert et al., 1996) and calcite is preserved in sediments above the lysocline (defined at a constant depth of 3300 m), and dissolves below. The biotic carbon isotope code was adapted to also account for these processes.

6 Summary

We have developed carbon isotope tracers in the ocean model of the CESM. The details of the implementation are described here in order to serve as reference for future users of these new model features and/or for model developers planning to modify the code. A comparison of the simulation results from the coarse nominal-3° resolution ocean model with present-day data for $\Delta^{14}C$ and $\delta^{13}C$ shows that the simulated carbon isotopes can represent the large-scale features of the observed distributions as well as the anthropogenic changes due to nuclear bomb tests and the burning of fossil fuels. The carbon isotopes also reveal some model biases, for example a too sluggish ventilation of the deep Pacific Ocean. Once a fast-spin up technique for the biotic carbon isotopes has been implemented, we are planning to further validate the model simulation in the fully-coupled CESM framework at 1° resolution. Ultimately, we plan to use the carbon isotopes for both present-day and paleo simulations in the fully-coupled framework of the CESM at the standard nominal 1° resolution in the ocean, in order to

GMDD
7, 7461–7503, 2014

investigate details of changes in the ocean circulation over the 20th century, the last Millennium, and at the Last Glacial Maximum.

Code availability

The carbon isotope code and the ecosystem driver code for CESM1.2 has been added to the ocean development trunk in the CESM SVN repository and is targeted for public release as part of the CESM1.3 in 2015. At that point the code will be available through the CESM1.3 release website at https://www2.cesm.ucar.edu/models/current. Prior to the release, developer access can already be applied for at https://www2.cgd.ucar.edu/sections/cseg/development-code.

Acknowledgements. A. Jahn was funded under the DOE SciDAC grant "Development of an Isotope-Enabled CESM for Testing Abrupt Climate Changes" (DE-SC0006744). We thank Michael Levy (NCAR) and David M. Hall (CU Boulder) for software engineering advice, Matt Long (NCAR) for helpful discussions, and Heather Graven (Scripps) for sharing her extensions of the OCMIP atmospheric $\Delta^{14}C$, $\delta^{13}C$, and CO_2 data with us. NCAR is sponsored by the National Science Foundation. N. Gruber and X. Giraud acknowledge funding from ETH Zürich. Computing resources (ark:/85065/d7wd3xhc) were provided by the Climate Simulation Laboratory at NCAR's Computational and Information Systems Laboratory on Yellowstone (2012), sponsored by the National Science Foundation and other agencies. Data analysis was performed with NCL Version 6.2.0 (2014).

References

Bacastow, R. B., Keeling, C. D., Lueker, T. J., Wahlen, M., and Mook, W. G.: The ^{13}C Suess Effect in the world surface oceans and its implications for oceanic uptake of CO_2: analysis of observations at Bermuda, Global Biogeochem. Cy., 10, 335–346, doi:10.1029/96GB00192, 1996. 7484

Bardin, A., Primeau, F., and Lindsay, K.: An offline implicit solver for simulating prebomb radiocarbon, Ocean Model., 73, 45–58, doi:10.1016/j.ocemod.2013.09.008, 2014. 7463, 7479

GMDD
7, 7461–7503, 2014

Bigeleisen, J.: The effects of isotopic substitutions on the rate of chemical reactions, J. Phys. Chem., 56, 823–828, 1952. 7471

Bohlen, L., Dale, A., and Wallmann, K.: Simple transfer functions for calculating benthic fixed nitrogen losses and C : N : P regeneration ratios in global biogeochemical models, Global Biogeochem. Cy., 26, GB3029, doi:10.1029/2011GB004198, 2012. 7485

Broecker, W. S. and Peng, T.-H.: Stratospheric contribution to the global bomb radiocarbon inventory: model versus observation, Global Biogeochem. Cy., 8, 377–384, doi:10.1029/94GB00680, 1994. 7495

Broecker, W. S., Peng, T. H., and Engh, R.: Modelling the carbon system, Radiocarbon, 22, 377–384, 1980. 7495

Broecker, W. S., Peng, T.-H., Östlund, G., and Stuiver, M.: The distribution of bomb radiocarbon in the ocean, J. Geophys. Res, 90, 6953–6970, doi:10.1029/JC090iC04p06953, 1985. 7479, 7495

Broecker, W. S., Sutherland, S., Smethie, W., Peng, T. H., and Östlund, G.: Oceanic radiocarbon: separation of the natural and bomb components, Global Biogeochem. Cy., 9, 263–288, doi:10.1029/95GB00208, 1995. 7479, 7495

Craig, H.: Carbon 13 is plants and the relationship between carbon 13 and carbon 14 variations in nature, J. Geol., 62, 115–149, 1954. 7471

Craig, H.: Isotopic standards for carbon and oxygen and correction factors for mass-spectrometric analysis of carbon dioxide, Geochim. Cosmochim. Ac., 12, 133–149, 1957. 7470

Crucifix, M.: Distribution of carbon isotopes in the glacial ocean: a model study, Paleoceanography, 20, PA4020, doi:10.1029/2005PA001131, 2005. 7463, 7464

Curry, W. B. and Oppo, D. W.: Glacial water mass geometry and the distribution of $\delta^{13}C$ of pCO_2 in the Western Atlantic Ocean, Paleoceanography, 20, PA1017, doi:10.1029/2004PA001021, 2005. 7462, 7463

Doney, S. C., Lindsay, K., Caldeira, K., Campin, J., Drange, H., Dutay, J., Follows, M., Gao, Y., Gnanadesikan, A., Gruber, N., Ishida, A., Joos, F., Madec, G., Maier-Reimer, E., Marshall, J., Matear, R., Monfray, P., Mouchet, A., Najjar, R., Orr, J., Plattner, G., Sarmiento, J., Schlitzer, R., Slater, R., Totterdell, I., Weirig, M., Yamanaka, Y., and Yool, A.: Evaluating global ocean carbon models: the importance of realistic physics, Global Biogeochem. Cy., 18, GB3017, doi:10.1029/2003GB002150, 2004. 7463

GMDD
7, 7461–7503, 2014

Dunne, J. P., Sarmiento, J. L., and Gnanadesikan, A.: A synthesis of global particle export from the surface ocean and cycling through the ocean interior and on the seafloor, Global Biogeochem. Cy., 21, GB4006, doi:10.1029/2006GB002907, 2007. 7485

Fiadiero, M. E.: Three-dimensional modeling of tracers in the deep Pacific Ocean: radiocarbon and the circulation, J. Mar. Res., 40, 537–550, 1982. 7466

Galbraith, E. D., Kwon, E. Y., Gnanadesikan, A., Rodgers, K. B., Griffies, S. M., Bianchi, D., Sarmiento, J. L., Dunne, J. P., Simeon, J., Slater, R. D., Wittenberg, A. T., and Held, I. M.: Climate variability and radiocarbon in the CM2Mc Earth System Model, J. Climate, 24, 4230–4254, doi:10.1175/2011JCLI3919.1, 2011. 7464

Godwin, H.: Half life of radiocarbon, Nature, 195, 984, doi:10.1038/195984a0, 1962. 7463, 7470

Goericke, R., Montoya, J. P., and Fry, B.: Physiology of isotopic fractionation in algae and cyanobacteria, in: Stable Isotopes in Ecology and Environmental Science, edited by: Lajtha, K. and Michener, R. H., Blackwell Scientific Publications, Oxford, 187–221, 1994. 7474

Graven, H. D., Gruber, N., Key, R., Khatiwala, S., and Giraud, X.: Changing controls on oceanic radiocarbon: new insights on shallow-to-deep ocean exchange and anthropogenic CO_2 uptake, J. Geophys. Res., 117, C10005, doi:10.1029/2012JC008074, 2012. 7463, 7464, 7466, 7479

Gruber, N. and Keeling, C. D.: The isotopic air–sea disequilibrium and the oceanic uptake of CO_2, in: Proceedings of the 2nd International Symposium CO_2 in the oceans, NIS, Tsukuba, Japan, edited by: Nojiri, Y., CGER-I037, Center for Global Environmental Research, National Institute for Environmental Studies, 245–250, 1999. 7501

Gruber, N. and Keeling, C.: An improved estimate of the isotopic air–sea disequilibrium of CO_2: implications for the oceanic uptake of anthropogenic CO_2, Geophys. Res. Lett., 28, 555–558, 2001. 7463, 7501

Gruber, N., Keeling, C. D., Bacastow, R. B., Guenther, P. R., Leuker, T. J., Wahlen, M., Meijer, H. A. J., Mook, W. G., and Stocker, T. F.: Spatiotemporal patterns of carbon-13 in the global surface oceans and the oceanic Suess effect, Global Biogeochem. Cy., 13, 307–335, 1999. 7463, 7484

Hesse, T., Butzin, M., Bickert, T., and Lohmann, G.: A model-data comparison of $\delta^{13}C$ in the glacial Atlantic Ocean, Paleoceanography, 26, PA3220, doi:10.1029/2010PA002085, 2011. 7464

GMDD
7, 7461–7503, 2014

Hesshaimer, V., Heimann, M., and Levin, I.: Radiocarbon evidence for a smaller oceanic carbon dioxide sink than previously believed, Nature, 370, 201–203, doi:10.1038/370201a0, 1994. 7479, 7495

Hurrell, J., Holland, M. M., Ghan, P. R. G. S., Kushner, J.. K. P., Lamarque, J.-F., Large, W. G., D. Lawrence, D., Lindsay, K., Lipscomb, W. H., Long, M., Mahowald, N., Marsh, D., Neale, R., Rasch, P., Vavrus, S., Vertenstein, M., Bader, D., Collins, W. D., Hack, J. J., Kiehl, J., and Marshall, S.: The Community Earth System Model: a framework for collaborative research, B. Am. Meteorol. Soc., 94, 1339–1360, doi:10.1175/BAMS-D-12-00121.1, 2013. 7463, 7465

Karlen, I., Olsson, I. U., Kallburg, P., and Kilici, S.: Absolute determination of the activity of two ^{14}C dating standards, Ark. Geofys., 4, 465–471, 1968. 7465, 7470

Keeling, C. D., Bacastow, R. B., and Tans, P. P.: Predicted shift in the $^{13}C/^{12}C$ ratio of atmospheric carbon dioxide, Geophys. Res. Lett., 7, 505–508, doi:10.1029/GL007i007p00505, 1980. 7463

Keller, K. and Morel, F. M. M.: A model of carbon isotopic fractionation and active carbon uptake in phytoplankton, Mar. Ecol.-Prog. Ser., 182, 295–298, 1999. 7473, 7481, 7482, 7483, 7494, 7501, 7502

Key, R. M., Kozyr, A., Sabine, C. L., Lee, K., Wanninkhof, R., Bullister, J. L., Feely, R. A., Millero, F. J., Mordy, C., and Peng, T.-H.: A global ocean carbon climatology: results from Global Data Analysis Project (GLODAP), Global Biogeochem. Cy., 18, GB4031, doi:10.1029/2004GB002247, 2004. 7463, 7478, 7479, 7480, 7495, 7497, 7498, 7499

Large, W. G. and Yeager, S. G.: The global climatology of an interannually varying air–sea flux data set, Clim. Dynam., 33, 341–364, doi:10.1007/s00382-008-0441-3, 2009. 7465, 7476

Lassey, K. R., Manning, M. R., and O'Brien, B. J.: An overview of oceanic radiocarbon: its inventory and dynamics, CRC Rev. Aquatic Sci., 3, 117–146, 1990. 7495

Laws, E. A., Bidigare, R. R., and Popp, B. N.: Effect of growth rate and CO_2 concentration on carbon isotopic fractionation by the marine diatom *Phaeodactylum tricornutum*, Limnol. Oceanogr., 42, 1552–1560, 1997. 7473

Laws, E. A., Popp, B. N., Bidigare, R. R., Kennicutt, M. C., and Macko, S. A.: Dependence of phytoplankton carbon isotopic composition on growth rate and $[CO_2]$aq: theoretical considerations and experimental results, Geochim. Cosmochim. Ac., 59, 1131–1138, doi:10.1016/0016-7037(95)00030-4, 1995. 7473, 7481, 7482, 7483, 7501, 7502

Libby, W. F.: Radiocarbon Dating, 2nd edn., Univ. Chicago Press, 1955. 7470

GMDD
7, 7461–7503, 2014

Marchal, O., Stocker, T. F., and Joos, F.: A latitude-depth, circulation-biogeochemical ocean model for paleoclimate studies. Development and sensitivities, Tellus B, 50, 290–316, doi:10.1034/j.1600-0889.1998.t01-2-00006.x, 1998. 7463

Matsumoto, K., Sarmiento, J. L., Key, R. M., Aumont, O., Bullister, J. L., Caldeira, K., Campin, J., Doney, S. C., Drange, H., Dutay, J.-C., Follows, M., Gao, Y., Gnanadesikan, A., Gruber, N., Ishida, A., Joos, F., Lindsay, K., Maier-Reimer, E., Marshall, J., Matear, R., Monfray, P., Mouchet, A., Najjar, R., Plattner, G., Schlitzer, R., Slater, R., Swathi, P., Totterdell, I., Weirig, M., Yamanaka, Y., Yool, A., and Orr, J.: Evaluation of ocean carbon cycle models with data-based metrics, Geophys. Res. Lett., 31, L07303, doi:10.1029/2003GL018970, 2004. 7463

McDermott, F.: Palaeo-climate reconstruction from stable isotope variations in speleothems: a review, Quaternary Sci. Rev., 23, 901–918, doi:10.1016/j.quascirev.2003.06.021, 2004. 7462

McNeil, B. I., Matear, R. J., and Tilbrock, B.: Does carbon 13 track anthropogenic CO_2 in the Southern Ocean?, Global Biogeochem. Cy., 15, 597–613, 2001. 7484

Meissner, K. J.: Younger Dryas: a data to model comparison to constrain the strength of the overturning circulation, Geophys. Res. Lett., 34, L21705, doi:10.1029/2007GL031304, 2007. 7463

Meissner, K. J., Schmittner, A., Weaver, A. J., and Adkins, J. F.: Ventilation of the North Atlantic Ocean during the Last Glacial Maximum: a comparison between simulated and observed radiocarbon ages, Paleoceanography, 18, 1023, doi:10.1029/2002PA000762, 2003. 7463, 7464

Mook, W. G.: ^{13}C in atmospheric CO_2, Neth. J. Sea Res., 20, 211–223, 1986. 7485

Moore, J. K., Lindsay, K., Doney, S. C., Long, M. C., and Misumi, K.: Marine ecosystem dynamics and biogeochemical cycling in the Community Earth System Model [CESM1(BGC)]: comparison of the 1990s with the 2090s under the RCP4.5 and RCP8.5 scenarios, J. Climate, 26, 9291–9312, doi:10.1175/JCLI-D-12-00566.1, 2013. 7470

Naegler, T.: Reconciliation of excess ^{14}C-constrained global CO_2 piston velocity estimates, Tellus B, 61, 372–384, 2009. 7463, 7466, 7479, 7480, 7481, 7495

Naegler, T. and Levin, I.: Closing the global radiocarbon budget 1945–2005, J. Geophys. Res., 111, D12311, doi:10.1029/2005JD006758, 2006. 7495

GMDD
7, 7461–7503, 2014

Naegler, T., Ciais, P., Rodgers, K., and Levin, I.: Excess radiocarbon constraints on air–sea gas exchange and the uptake of CO_2 by the oceans, Geophys. Res. Lett., 33, L11802, doi:10.1029/2005GL025408, 2006. 7463, 7466, 7479, 7495

NCL Version 6.2.0, Boulder, C. U.: The NCAR Command Language, doi:10.5065/D6WD3XH5, 2014. 7486

O'Leary, M. H.: Measurement of the isotope fractlonation associated with diffusion of carbon dioxide in aqueous solution, J. Phys. Chem., 88, 823–825, 1984. 7474

Orr, J. C.: Global Ocean Storage of Anthropogenic Carbon (GOSAC), Tech. rep., EC Environment and Climate Program, Final Report, 2002. 7463, 7464

Orr, J., Najjar, R., Sabine, C., and Joos, F.: Abiotic-HOWTO, Technical report, revision: 1.16, available at: http://ocmip5.ipsl.jussieu.fr/OCMIP/phase2/simulations/Abiotic/HOWTO-Abiotic.html (last access: 15 May 2012), 2000. 7464, 7465, 7466, 7476, 7477

Peacock, S.: Debate over the ocean bomb radiocarbon sink: closing the gap, Global Biogeochem. Cy., 18, GB2022, doi:10.1029/2003GB002211, 2004. 7479, 7495

Petit, J. R., Jouzel, J., Raynaud, D., Barkov, N. I., Barnola, J.-M., Basile, I., Bender, M., Chappellaz, J., Davis, M., G, D., Delmotte, M., Kotlyakov, V. M., Legrand, M., Lipenkov, V. Y., Lorius, C., Pepin, L., Ritz, C., Saltzman, E., and Stievenard, M.: Climate and atmospheric history of the past 420,000 years from the Vostok ice core, Antarctica, Nature, 399, 429–436, 1999. 7462

Polka, J. S., van Beynenb, P., Asmeromc, Y., and Polyakc, V. J.: Reconstructing past climates using carbon isotopes from fulvic acids in cave sediments, Chem. Geol., 360–361, 1–9, doi:10.1016/j.chemgeo.2013.09.022, 2013. 7462

Popp, B. N., Laws, E. A., Ridigare, R. R., Dore, J. E., Hanson, K. L., and Wakeham, S. G.: Effect of phytoplankton cell geometry on carbon isotope fractionation, Geochim. Cosmochim. Ac., 62, 69–77, 1998. 7494

Quay, P. D., Tilbrook, B., and Wong, C. S.: Oceanic uptake of fossil fuel CO_2: carbon-13 evidence, Science, 256, 74–79, 1992. 7463, 7484

Rau, G. H., Takahashi, T., and Marais, D. J. D.: Latitudinal variations in plankton $\delta^{13}C$: implications for CO_2 and productivity in past oceans, Nature, 341, 516–518, 1989. 7473, 7481, 7482, 7483, 7501, 7502

Raymond, P. A., Bauerb, J. E., Caracoc, N. F., Colec, J. J., Longworthd, B., and Petschd, S. T.: Controls on the variability of organic matter and dissolved inorganic carbon ages in northeast US rivers, Mar. Chem., 92, 353–366, 2004. 7485

GMDD
7, 7461–7503, 2014

Schmittner, A., Gruber, N., Mix, A. C., Key, R. M., Tagliabue, A., and Westberry, T. K.: Biology and air–sea gas exchange controls on the distribution of carbon isotope ratios ($\delta^{13}C$) in the ocean, Biogeosciences, 10, 5793–5816, doi:10.5194/bg-10-5793-2013, 2013. 7463, 7464, 7478, 7482, 7483, 7497, 7498, 7499, 7500, 7501, 7502

Shields, C. A., Bailey, D. A., Danabasoglu, G., Jochum, M., Kiehl, J. T., Levis, S., and Park, S.: The low-resolution CCSM4, J. Climate, 25, 3993–4014, doi:10.1175/JCLI-D-11-00260.1, 2012. 7465

Sikes, C. S., Roer, R. D., and Wilbur, K. M.: Photosynthesis and coccolith formation: inorganic carbon sources and net inorganic reaction of deposition, Limnol. Oceanogr., 25, 248–261, 1980. 7473

Soetaert, K., Herman, P. M. J., and Middelburg, J. J.: A model of early diagenetic processes from the shelf to abyssal depths, Geochim. Cosmochim. Ac., 60, 1019–1040, doi:10.1016/0016-7037(96)00013-0, 1996. 7485

Sonnerup, R. E., Quay, P. D., McNichol, A. P., Bullister, J. L., Westby, T. A., and Anderson, H. L.: Reconstructing the ocean ^{13}C Suess effect, Global Biogeochem. Cy., 13, 857–872, doi:10.1029/1999GB900027, 1999. 7463, 7484

Stuiver, M. and Polach, H. A.: Discussion: reporting of ^{14}C Data, Radiocarbon, 19, 355–363, 1977. 7470

Sweeney, C., Gloor, E., Jacobson, A. R., Key, R. M., McKinley, G., Sarmiento, J. L., and Wanninkhof, R.: Constraining global air–sea gas exchange for CO_2 with recent bomb ^{14}C measurements, Global Biogeochem. Cy., 21, GB2015, doi:10.1029/2006GB002784, 2007. 7463, 7466, 7479, 7495

Tagliabue, A. and Bopp, L.: Towards understanding global variability in ocean carbon-13, Global Biogeochem. Cy., 22, GB1025, doi:10.1029/2007GB003037, 2008. 7464, 7484

Toggweiler, J. R., Dixon, K., and Bryan, K.: Simulations of radiocarbon in a coarse-resolution world ocean model 1. Steady state prebomb distributions, J. Geophys. Res., 94, 8217–8242 doi:10.1029/JC094iC06p08217, 1989. 7463, 7466, 7468

Tortell, P. D., Reinfelder, J. R., and More, F. M. M.: Active uptake or bicarbonate by diatoms, Nature, 390, 243–244, 1997. 7473

Turner, J. V.: Kinetic fractionation of ^{13}C during calcium carbonate precipitation, Geochim. Cosmochim. Ac., 46, 1183–1191, doi:10.1016/0016-7037(82)90004-7, 1982. 7474

Wanninkhof, R.: Relationship between wind speed and gas exchange over the ocean, J. Geophys. Res., 97, 7373–7382, 1992. 7463, 7466, 7468, 7479

GMDD
7, 7461–7503, 2014

Waugh, D. W., Hall, T. M., and Haine, T. W. N.: Relationships among tracer ages, J. Geophys. Res., 108, 3138, doi:10.1029/2002JC001325, 2003. 7463

Yellowstone: Computational and Information Systems Laboratory, National Center for Atmospheric Research, Boulder, CO, Yellowstone: IBM iDataPlex System (Climate Simulation Laboratory), available at: http://n2t.net/ark:/85065/d7wd3xhc (last access: 15 September 2014), 2012. 7486

Zeebe, R. E. and Wolf-Gladrow, D.: CO_2 in Seawater: Equilibrium, Kinetic, Isotopes, 3rd Edn., Elsevier Oceanography Series 65, Elsevier Ltd, 2001. 7474

Zhang, J., Quay, P. D., and Wilbur, D. O.: Carbon isotope fractionation during gas-water exchange and dissolution of CO_2, Geochim. Cosmochim. Ac., 59, 107–114, 1995. 7471

Ziveri, P., Stoll, H. M., Probert, I., Klaas, C., Geisen, M., J. J. Y., and Ganssen, G.: Stable isotope vital effects in coccolith calcite, Earth Planet. Sc. Lett., 210, 137–149, 2003. 7474

GMDD
7, 7461–7503, 2014

Table 1. Parameters using in the parameterization of ϵ_p for the implementation following Keller and Morel (1999). The values for small phytoplankton are based on *E. huxleyi*, the value for diatoms are based on *P. tricornumtum*, and the values for diatoms are based on based on *Synechococcus* sp. (Keller and Morel, 1999; Popp et al., 1998).

	Small phytoplankton	Diatom	Diazotroph
Qc [mol C cell^{-1}]	69.2×10^{-14}	63.3×10^{-14}	3×10^{-14}
cell$_{permea}$ [m s^{-1}]	1.8×10^{-5}	3.3×10^{-5}	3.0×10^{-8}
cell$_{surf}$ [m^2]	87.6×10^{-12}	100.6×10^{-12}	5.8×10^{-12}
C_{up}	2.2	2.3	7.5
ϵ_{fix}	25.3	26.6	30

GMDD
7, 7461–7503, 2014

Table 2. Excess oceanic radiocarbon inventory, measured in 10^{26} atoms of ^{14}C, from various sources for 1975 (GEOSECS) and 1995 (WOCE). Corrections by Naegler et al. (2006) are for neglected ocean regions, corrections by Naegler (2009) are for neglected contributions from increasing DIC. The values from this study are listed at the bottom, for the abiotic and biotic implementation. The biotic excess radiocarbon inventories are the same for all biological fractionation choices tested.

Publication	1975 (GEOSECS)	1995 (WOCE)
Broecker et al. (1980)	314 ± 35	
Broecker et al. (1985)	289	
Lassey et al. (1990)	303	
Hesshaimer et al. (1994)	225	
Broecker and Peng (1994)	300	
Broecker et al. (1995)	305 ± 30	
Peacock (2004) multitracer correlation	241 ± 60	335 ± 15
corrected by Naegler et al. (2006)	245 ± 60	340 ± 15
corrected by Naegler (2009)	252 ± 60	367 ± 15
Peacock (2004) silicate approach	262 ± 26	
corrected by Naegler et al. (2006)	264 ± 26	
Key et al. (2004)		313 ± 47
corrected by Naegler et al. (2006)		355 ± 50
corrected by Naegler (2009)		383 ± 50
Naegler and Levin (2006)	258 ± 13	367 ± 17
Sweeney et al. (2007)	225	343 ± 40
corrected by Naegler (2009)	232	370 ± 40
Naegler (2009)		373 ± 98
This study, abiotic ^{14}C	286	372
This study, biotic ^{14}C	291	384

GMDD
7, 7461–7503, 2014

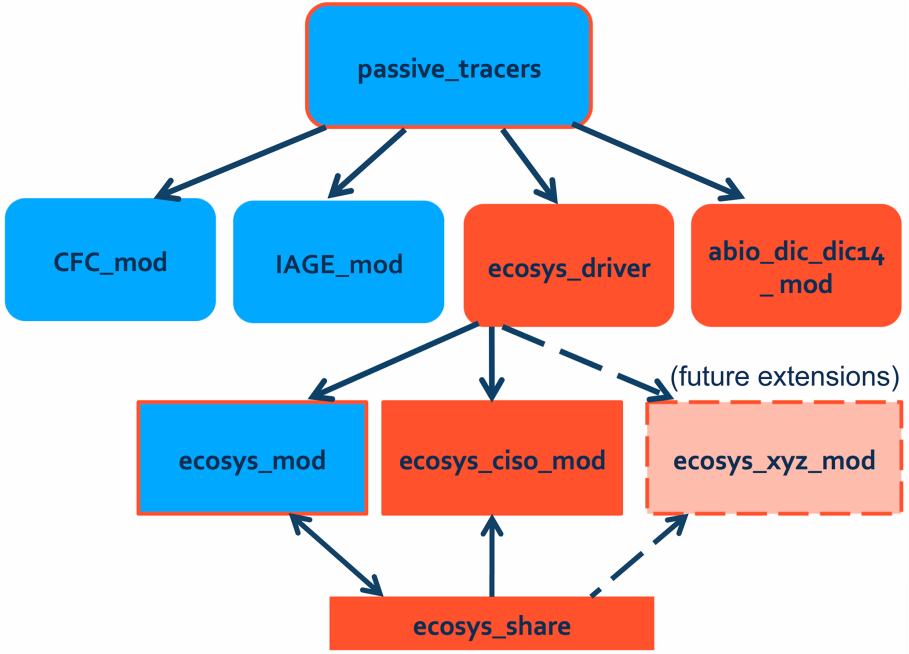

Figure 1. Schematic of the passive tracer modules with the new ecosystem driver and carbon isotope modules. Existing modules are shown in blue, new modules are shown in red, and edited modules are shown in blue with a red box. Dashed lines indicate future developments. This schematic shows how the ecosystem driver acts as an interface between the ecosystem-related modules and the passive tracers module that drives all tracer modules as well as how `ecosys_share` is used to share variables computed by the ecosystem model and used by other modules beside the ecosystem model.

GMDD
7, 7461–7503, 2014

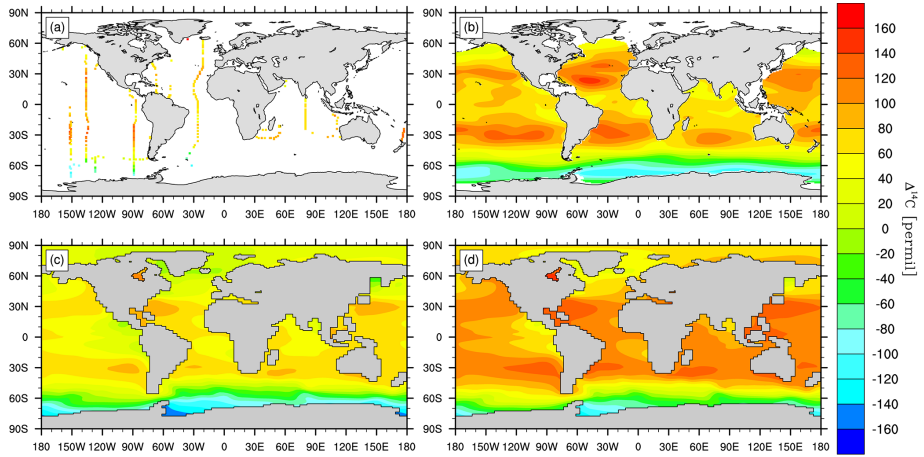

Figure 2. Surface values of total $\Delta^{14}C$ from the 1990s (including bomb ^{14}C) from **(a)** cruise data compiled by Schmittner et al. (2013), **(b)** the gridded GLODAP data (Key et al., 2004), **(c)** simulated biotic $\Delta^{14}C$, and **(d)** simulated abiotic $\Delta^{14}C$.

GMDD
7, 7461–7503, 2014

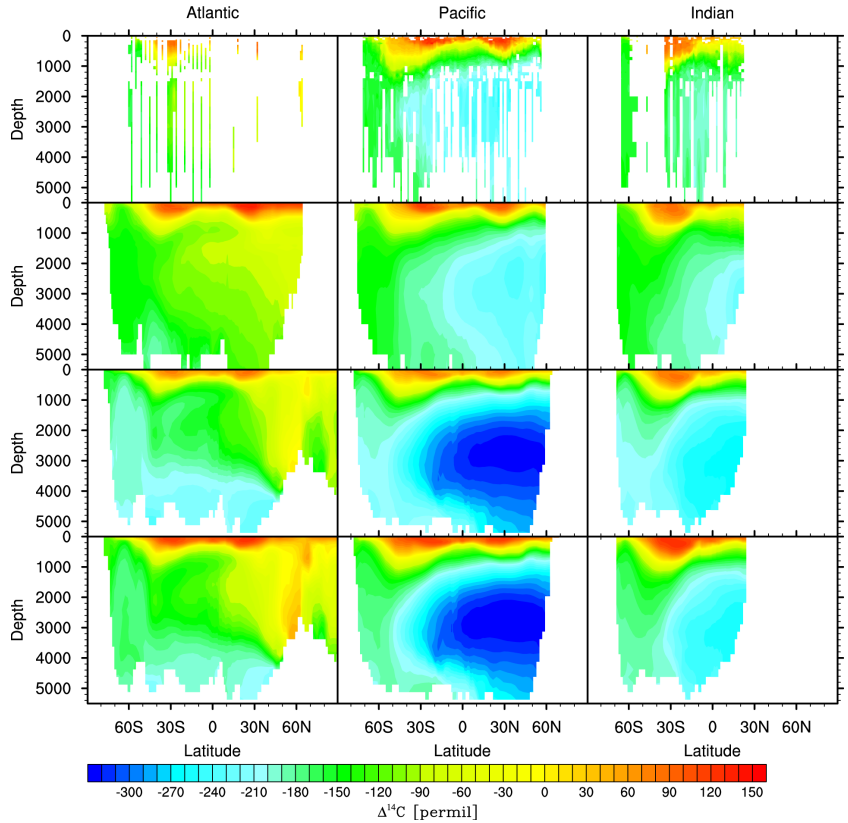

Figure 3. Zonal averages of total $\Delta^{14}C$ for the Atlantic, Pacific, and Indian Ocean for the 1990s, from cruise data compiled by Schmittner et al. (2013) (top row), the gridded GLODAP data (Key et al., 2004) (second row), the $\Delta^{14}C$ from the biotic model (third row), and the abiotic model (bottom row). Note that due to the sparse observational data (see Fig. 2a for the coverage at the surface), the zonal average from the cruise data in the top row is more of a zonal composite than a zonal average.

GMDD
7, 7461–7503, 2014

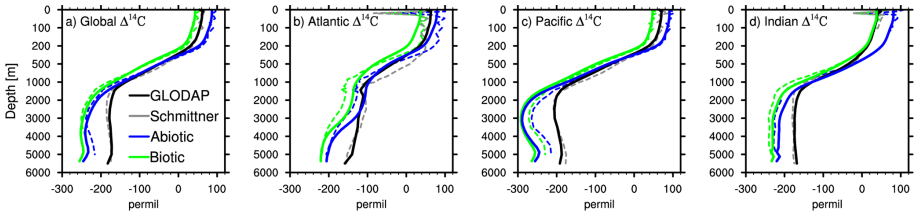

Figure 4. Depth profiles of $\Delta^{14}C$ for **(a)** the global ocean, **(b)** the Atlantic Ocean, **(c)** the Pacific Ocean, and **(d)** the Indian Ocean. The simulated biotic (green) and abiotic (blue) $\Delta^{14}C$ is compared to the global gridded GLODAP $\Delta^{14}C$ (black) dataset (Key et al., 2004). In addition dashed lines show the cruise data compiled by Schmittner et al. (2013) (gray) and the model simulated data subsampled at the same locations as this data (green and blue dashed lines).

GMDD
7, 7461–7503, 2014

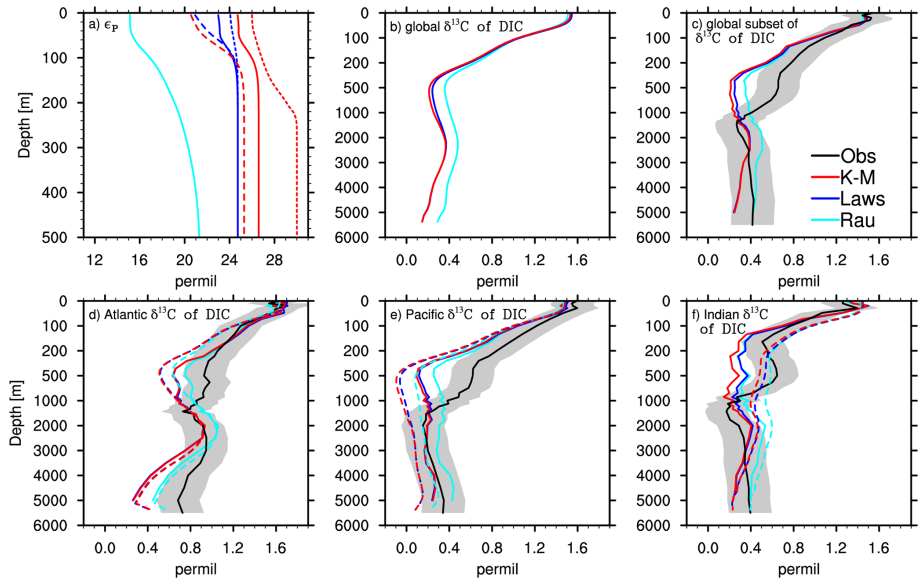

Figure 5. (a) Depth profiles over the top 500 m (where ϵ_p is important because of primary production) of the globally-averaged values of ϵ_p produced by the three tested parameterizations for biological fractionation for diatoms (solid line), diazotrophs (short dashes), and small phytoplancton (large dashes). The simulated globally-averaged depth profile (0–6000 m) of $\delta^{13}C_{DIC}$ in the 1990s is shown in **(b)**, and the global average depth profile of the subset model $\delta^{13}C_{DIC}$ for the same grid points as in the cruise data compiled by Schmittner et al. (2013) is shown in **(c)**. Basin average depth-profiles are shown in **(d–f)**, with dashed lines showing the full basin average from the model and solid lines showing the subset averages for the same points as the cruise data compiled by Schmittner et al. (2013). The uncertainty for the cruise data is shown as grey shading in **(c)**, and is ±0.2 ‰ (Schmittner et al., 2013). Note that the irregular *y* axis in **(b–f)** emphasizes the upper ocean.

GMDD
7, 7461–7503, 2014

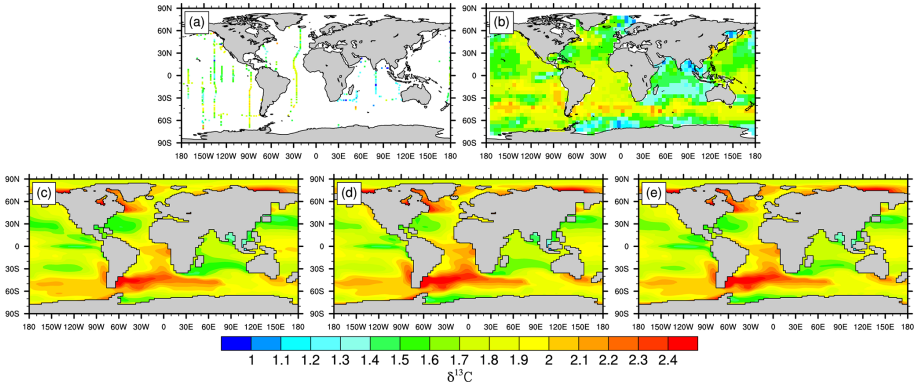

Figure 6. Surface values of δ^{13}C for the 1990s from **(a)** cruise data compiled by Schmittner et al. (2013), **(b)** 5° extrapolated gridded data from Gruber and Keeling (1999) and Gruber and Keeling (2001), and **(c–e)** the biotic model, using the biological fractionation from **(c)** Rau et al. (1989), **(d)** Laws et al. (1995), and **(e)** Keller and Morel (1999).

GMDD
7, 7461–7503, 2014

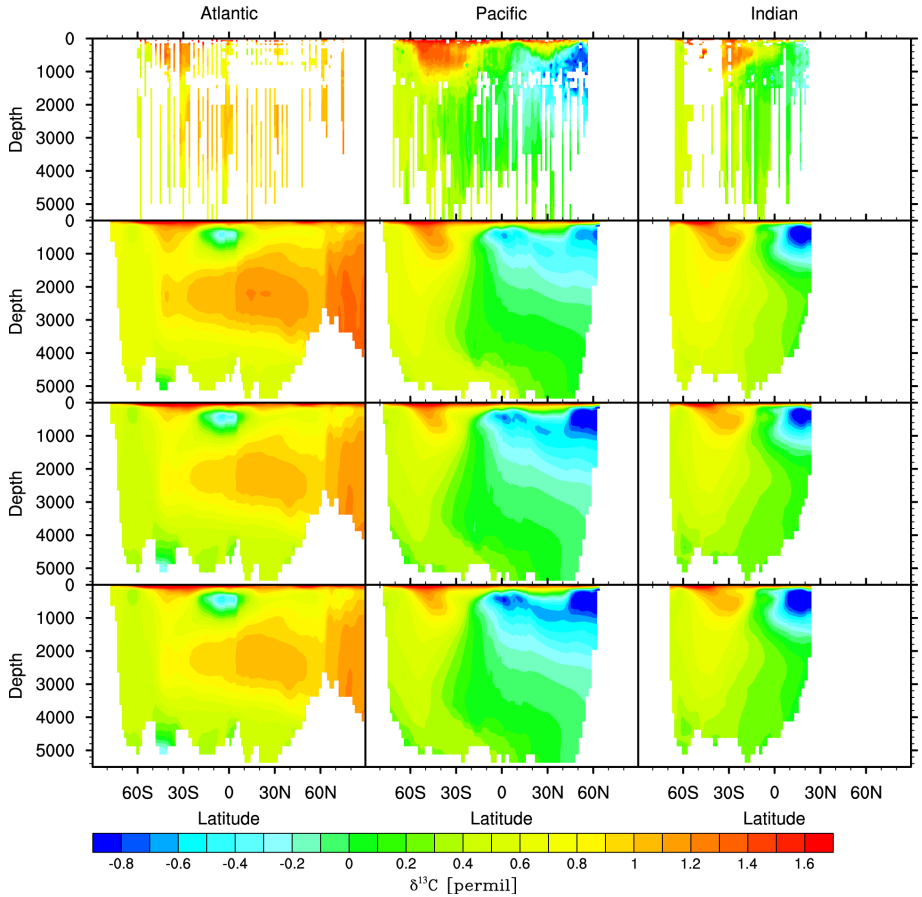

Figure 7. Zonal ocean basin composites from the cruises data compiled by Schmittner et al. (2013) (top row), compared to 1990s zonal basin averages from the model simulation using the biological fractionation from Rau et al. (1989) (second row), Laws et al. (1995) (third row), and Keller and Morel (1999) (bottom row).

GMDD
7, 7461–7503, 2014

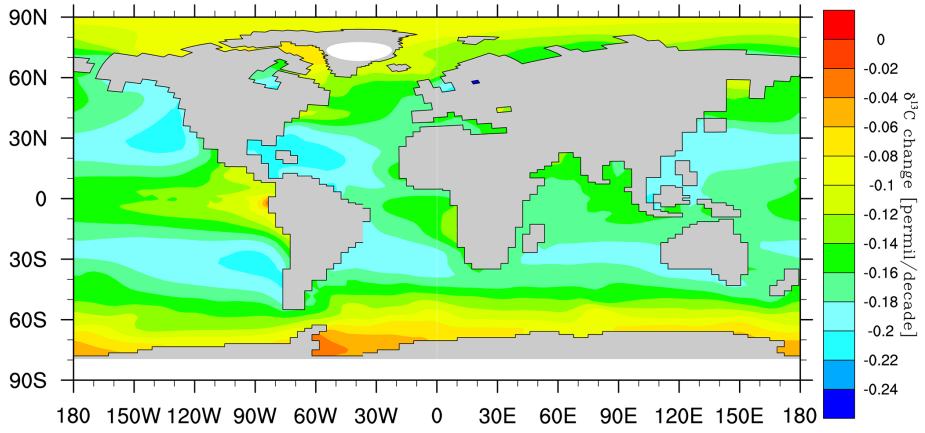

Figure 8. Surface ocean Suess effect (the change in $\delta^{13}C$) between 1970 and 1990, in ‰ decade^{-1}.

GMDD
7, 7461–7503, 2014